




Article

Ammonium Hydroxide Mediated Hydrothermal Crystallization of Hydroxyapatite Coatings on Titanium Substrate

Katarzyna Suchanek ^{1,*} , Marcin Perzanowski ², Janusz Lekki ² , Martyna Strąg ³ and Marta Marszałek ² 

¹ Institute of Physics, Cracow University of Technology, Podchorążych 1, 30-084 Kraków, Poland

² The Institute of Nuclear Physics Polish Academy of Sciences, Radzikowskiego 152, 31-342 Krakow, Poland; marcin.perzanowski@ifj.edu.pl (M.P.); Janusz.Lekki@ifj.edu.pl (J.L.); marta.marszalek@ifj.edu.pl (M.M.)

³ The Institute of Metallurgy and Materials Science Polish Academy of Sciences, Reymonta 25, 30-059 Krakow, Poland; martynastrag@gmail.com

* Correspondence: katarzyna.suchanek@pk.edu.pl; Tel.: (+48-12)-637-06-66

Received: 1 February 2019; Accepted: 15 March 2019; Published: 19 March 2019



Abstract: Controlled growth of hydroxyapatite (HAp) coatings on titanium substrate plays an important role in the fabrication of the composites for bone tissue engineering. We describe the synthesis of the crystalline hydroxyapatite coatings on the Ti/TiO₂ substrate through a hydrothermal method by using ethylenediamine tetraacetic acid disodium salt (Na₂EDTA) and varying concentrations of ammonium hydroxide (NH₄OH) in calcium-phosphate precursor solution. Na₂EDTA serves as a chelating agent, while NH₄OH is used as an alkaline source and crystal growth modifier. We characterized the HAp coatings using x-ray diffraction, scanning electron microscopy, and Raman spectroscopy. We also performed the elemental chemical analysis by means of a particle induced x-ray emission method. Our results show that there is a pH limit for which the hydrothermal deposition of HAp on titanium occurs. Moreover, we observed that NH₄OH had a measurable influence on the coating thickness as well as on the size and shape of the HAp crystals. We found that with the increase of NH₄OH concentration, the thickness of the Hap layer increases and its morphology changes from irregular flakes to well-defined hexagonal rods.

Keywords: hydroxyapatite coatings; hydrothermal synthesis; ammonium hydroxide

1. Introduction

Calcium phosphates, in particular hydroxyapatite (HAp, Ca₁₀(PO₄)₆(OH)₂), form the mineral constituent of hard tissues [1]. HAp coatings on the titanium substrates have excellent biocompatibility and osteoconductivity, and therefore are widely applied in the correction of bone defects caused by traumas, diseases, and genetic disorders [2]. Geometrical factors such as shape and dimensions of HAp crystals have a significant impact on their biological response and mechanical properties under load bearing conditions [3,4]. Numerous deposition techniques of HAp on metallic substrates have been described, such as plasma spraying [5,6], electrophoresis [7], sol-gel [8], magnetron sputtering [9], and the hydrothermal method [10]. However, it is still a challenge to obtain HAp coatings with desirable properties, in particular HAp crystals with well-defined morphology and precisely adjustable sizes. Development of a method for controlled growth of the HAp coatings would help with the realization of the new concept of biomaterials: materials which regulate cellular responses and enhance bone mineralization.

The hydrothermal approach has been proven to be an effective and convenient process in preparing HAp powders. During the synthesis carried out in an autoclave at elevated temperature

and elevated pressure, crystalline HAp coatings with a Ca/P ratio close to the stoichiometric value were obtained [10]. Depending on the reaction mechanism, several pathways for hydrothermal crystallization of HAp can be distinguished, i.e.: (i) chelate decomposition [11–14], (ii) urea decomposition [15,16], (iii) dissolution–precipitation of calcium phosphate precursor [17,18], and others [19]. The chelate decomposition technique, used herein, is based on chemical precipitation of HAp phase from solution containing calcium and phosphate sources. Additionally, an organic modifier is added, usually a chelating agent such as ethylenediamine tetraacetic acid (EDTA), to adjust the concentration of free Ca^{2+} ions, and therefore to control the nucleation and growth of the HAp crystals [12–14,20]. At room temperature, EDTA immediately forms stable Ca-EDTA complex, depleting the stock solution of free Ca^{2+} ions. However, at hydrothermal conditions, i.e., increased temperature and pressure, the equilibrium state shifts towards the Ca-EDTA dissociation, releasing the Ca^{2+} ions and consequently the precipitation of calcium phosphate phase appears. Crystal growth during the hydrothermal process is regulated not only by the chelating agent, but also by the pH of the reacting solution. The pH affects the equilibrium state in the reacting medium and the solubility of the HAp phase. The impact of the complexing agent as well as of pH on the morphology of the HAp powders in chelate decomposition synthesis is well known [20–22]. HAp powders of flower-like nanostructures, nanorod aggregates, dumbbell-like nanostructures, hexagonal prism-like nanorods, whiskers, and nanowires can be obtained depending on the used reactants and surfactants. However, the effect of pH on the heterogeneous nucleation and growth of HAp coatings on the Ti/TiO₂ substrate is less understood. The process is, as described, complex and pH also influences the physicochemical properties of the Ti/TiO₂ surface on which HAp crystals nucleate and grow [23]. Pioneering research in this field was carried out by Fujishiro et al. [24,25]. These authors synthesized HAp on titanium and other metallic substrates using the chelate decomposition method and NaOH as alkalizing agent. As a result, plate-like monetite and needle-like hydroxyapatite crystals were obtained at pH < 7.0. The crystals were irregular in shape and the surface of the substrate was not homogeneously covered. Above this pH, the crystals did not grow. The application of the appropriate seeding layer made it possible to obtain a dense coating at a higher pH. More recently, adequate HAp crystal morphology in the coatings synthesized hydrothermally was obtained also through a suitable seeding layer [26–28]. Lu et al. showed that the use of the glass substrate with a ZnO seed layer leads to the oriented growth of the hydroxyapatite nanorod array [26]. Chen et al. fabricated HAp coatings with oriented nanorod arrays by using the bioglass as precursors [27]. Uniform, highly crystalline HAp coatings have also been deposited on grafted titanium substrate as shown by Shen et al. [28]. A self-assembly technique was applied to introduce functional groups on titanium which served as nucleation sites for apatite crystals.

In this study we investigate the effect of ammonia hydroxide concentration on the nucleation and growth of the HAp coatings on the Ti/TiO₂ substrate. The issue of the alkalizing agent seems to be important; as has been recently shown by Li et al. [29] the size of HAp particles could be controlled by alkaline reagent. We show that alkalinity adjusted by ammonia solution has measurable influence on the coatings thickness, and on the size and shape of HAp crystals, as well as on the crystal growth rate on the titanium surface.

2. Materials and Methods

2.1. Titanium Substrate Preparation

Commercially available pure titanium sheet (BIMO Metals, Wrocław, Poland) with a thickness of 3 mm was cut into square samples with dimensions of 10 × 10 mm². The samples were cleaned with acetone and alcohol in an ultrasonic bath and rinsed with ultrapure water (18.2 MΩ·cm⁻¹) from a Polwater system. The cleaned Ti plates were firstly soaked in a mixture of H₂SO₄ (6.3 mol·dm⁻³) and HCl (1.8 mol·dm⁻³) solution in a weight ratio of 1:1 at 70 °C for 1 h, then treated in oxidizing conditions

at 650 °C to form a TiO₂ layer according to the method described in reference [10]. The as-prepared Ti/TiO₂ substrates were further used for hydrothermal synthesis.

2.2. Chemical Synthesis

In a typical synthesis procedure calcium nitrate Ca(NO₃)₂ (0.2 mol·dm⁻³) and diammonium phosphate (NH₄)₂HPO₄ (0.12 mol·dm⁻³) were individually dissolved in ultrapure water. Ethylenediamine tetraacetic acid (EDTA) was added to the calcium solution as a chelating agent with fixed molar ratio of EDTA:Ca²⁺ (1:1). When the reactants were entirely mixed, the two solutions were combined and subsequently stirred at room temperature for 30 min. Next, the ammonium hydroxide (NH₄OH) was added drop-wise. To study the effect of pH variation on the HAp crystal growth, the molar concentration of NH₄OH was set to a specific value ranging from 0.2 to 1.34 mol·dm⁻³, causing pH changes from 6.0 to 10.5. The five final solutions were labelled as CaP_x (where x = 0.2, 0.27, 0.4, 0.8, 1.34, and denotes the NH₄OH concentration), transferred into 200 mL Teflon vessels and put into hydrothermal reactor (Carl Roth 2098.1). The titanium substrate was placed on a special holder at an angle of 45° to the bottom of the container. The holder was put inside the glass vessel in such a way that samples were completely immersed in the solution. The autoclave was sealed and set up to 200 °C for 7 h. After the synthesis samples were gently rinsed with ultrapure water and left to dry at room temperature.

2.3. Characterization

The surface morphology of the as-deposited HAp coatings was examined using scanning electron microscope (SEM, Tescan Vega 3). The crystal structure was determined with an x-ray diffractometer (XRD, PANalytical X'Pert Pro) operating at 30 mA and 40 kV. The radiation wavelength (Cu K_α) was 1.54 Å. X-ray diffraction patterns were taken over the 2θ range of 20°–80° with a 0.05° step size. The angular resolution of the instrument was calibrated using the LaB6 line profile standard (SRM660a-NIST certificate). The chemical composition of the HAp coatings was determined with Raman spectrometer (Almega XR of Thermo Electron Corp.). A 532 nm laser was used to excite the Raman signal. The data were recorded in the spectral range from 100 to 4000 cm⁻¹ with spectral resolution of 2 cm⁻¹. The elemental analysis was performed using energy dispersive x-ray spectrometer (QUANTAX EDS, Bruker) equipped with an XFlash 610M detector with the resolution of <129 eV for the Mn K_α line. Chemical composition of the samples was measured using particle induced x-ray emission (PIXE) technique. The μPIXE analysis was performed using 2 MeV protons from the electrostatic Van de Graaff accelerator, at the Institute of Nuclear Physics, Polish Academy of Sciences, Cracow (IFJ PAN). Rectangular areas (0.25 × 0.25 mm²) were scanned with the beam of approx. 20 μm in diameter. The semiconductor Si(Li) detector, with the resolution of 160 eV for the energy of 5.9 keV and the active area of 80 mm², was placed 25 mm away from the irradiated sample and was operating without any attenuation filter.

3. Results

Figure 1 shows SEM images of the Ti/TiO₂ surfaces after the hydrothermal treatment in calcium-phosphate precursor solution with various ammonium hydroxide molar concentrations. The development of hexagonal rods with well-defined geometry is clearly visible in the consecutive top view SEM images (Figure 1f–j). For sample with the lowest concentration of ammonia (CaP_x = 0.2), no crystal growth was observed on the Ti/TiO₂ surface (Figure 1f). At pH = 7.2 (CaP_x = 0.27), irregular HAp crystals in the form of plates were sparsely formed (Figure 1g). The width of plates varies from 0.1 to 0.8 μm. A further increase in pH led to the growth of HAp crystals with hexagonal symmetry. We observed the aggregated rods of about 0.35 μm in diameter for CaP_x = 0.4 (Figure 1h), for higher pH we observed the separate hexagonal rods with 0.55 μm in diameter (Figure 1i), and for the highest pH value we registered the well-defined hexagonal crystals of about 0.95 μm in diameter (Figure 1j). Figure 2a illustrates the diameters of hexagonal HAp crystals as a function of the pH value.

We also performed the cross-sectional SEM imaging which allowed us to estimate the thickness of the HAp coatings using the ImageJ open source program (Figure 1k–o). In these images the layered structure of the Ti/TiO₂/HAp systems is clearly visible. The results show that the pH of the reacting solution affects the crystal growth rate; the higher pH, the thicker is the HAp coating. The thickest hydroxyapatite coatings of approximately 50 μm were grown at pH = 10.5. The thicknesses of the HAp layers produced at various ammonia concentrations are summarized in Table 1 and shown in Figure 2a. The elemental distribution of each sample was analyzed by EDS spectrometry. The results are shown in Figure 1 a–e and are included in Table 1. EDS analysis of Ti/TiO₂/HAp structures confirmed the presence of Ca and P. The calculated Ca/P relative atomic ratio was 1.51, 1.57, 1.69 and 1.74 for CaP_x = 0.27, CaP_x = 0.4, CaP_x = 0.8 and CaP_x = 1.34, respectively. The Ca/P values for samples synthesized at pH ≥ 9.0 within the margin of experimental error are in good agreement with the theoretical data on the stoichiometry of the HAp phase. A minor deviation from the nominal composition observed for the CaP_x = 0.27 sample may suggest that the synthesized crystals contained more defects, or that the hydroxyapatite was calcium deficient. However, it should be noted that for this sample the calcium and phosphorus elemental content was very low.

Strong inhibition of crystal growth shown in the SEM image for low pH (pH < 7) could be due to the fact that the coating precipitation under hydrothermal conditions is a complex phenomenon and pH of the solution also affects the chemical nature of the Ti/TiO₂ substrate itself. We intentionally created the TiO₂ layer on Ti since the surface of titanium oxide in aqueous medium exhibits surface charge strongly depending on the pH of solution. Surface charge can promote crystal nucleation, and the electrostatic attraction may be the driving force for the nucleation process of HAp [30,31]. The isoelectric point (IEP) for TiO₂ varies between 5 and 6.5 depending on the crystal phase [32], which means that in the acidic environment (pH < 7), the adsorption of functional groups on titanium is limited. This effect is well demonstrated in SEM images: at low pH the HAp nucleation is limited, while a further increase in pH intensifies the crystal growth rate.

The crystal structure and phase purity of the HAp coatings were examined by XRD (Figure 3a). For sample prepared at pH = 6.0 we observed exclusively α-Ti and crystalline TiO₂ with the tetragonal rutile structure, originating from the substrate. For other samples, the XRD analysis indicated the presence of the hexagonal HAp phase with the space group P63/m, irrespective of the NH₄OH addition as a pH modifier. The calculated lattice parameters were a = 9.44(2) Å, c = 6.89(2) Å; these are in good agreement with the literature data [33]. No other calcium phosphate phases, such as TCP or OCP, were observed.

Table 1. Hydrothermal synthesis parameters; estimated HAp layer thickness.

Sample	NH ₄ OH Concentration [mol·dm ⁻³]	pH	HAp Layer Thickness Mean Value (SD) * (n = 6) [μm]	Ca/P Molar Ratio
CaP _x = 0.2	0.2	6.0	—	—
CaP _x = 0.27	0.27	7.2	16.5(2.4)	1.51(0.10)
CaP _x = 0.4	0.4	9.0	16.9(3.1)	1.57(0.10)
CaP _x = 0.8	0.8	10.0	29.5(1.3)	1.69(0.11)
CaP _x =1.34	1.34	10.5	48.2(5.2)	1.74(0.11)

* SD corresponds to standard deviation.

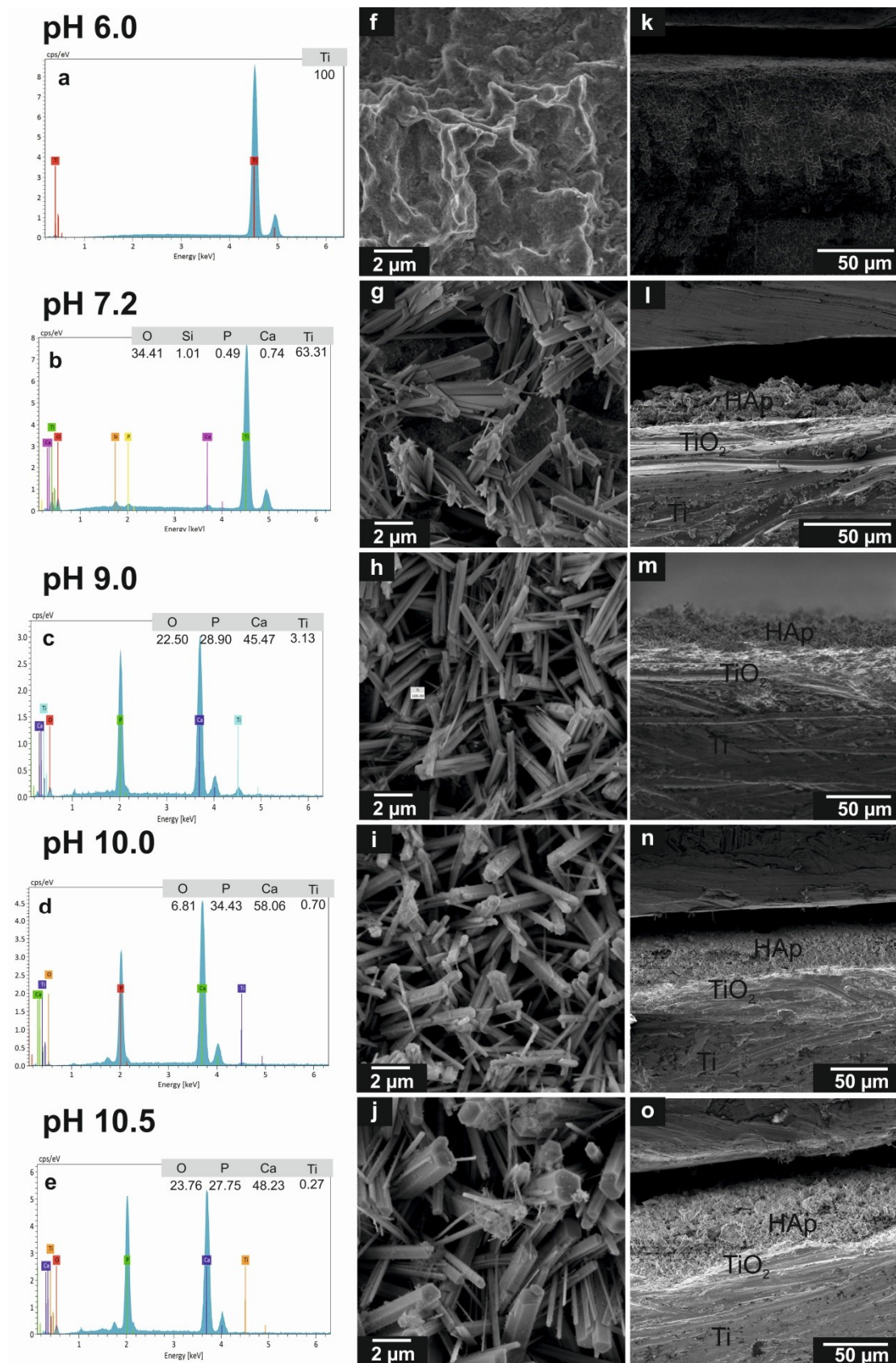


Figure 1. The morphological and elemental analysis of HAp coatings. (a–e) EDS spectra and (f–j) top view SEM images showing the morphological evolution of calcium phosphate crystals synthesized on Ti/TiO₂ through hydrothermal method for different ammonium hydroxide concentrations. Panels (k–o) show the cross-sectional images of HAp coatings synthesized at different pH.

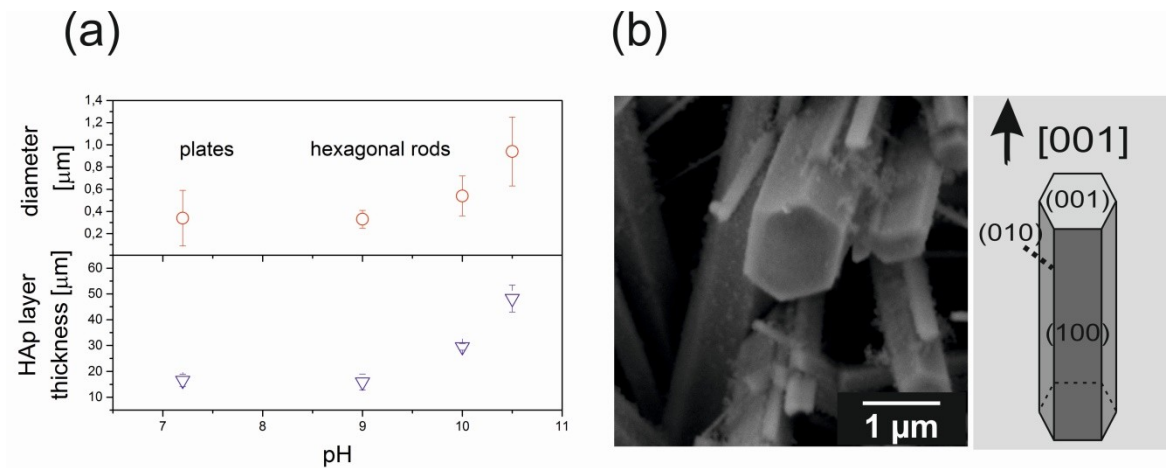


Figure 2. (a) Effect of ammonium hydroxide concentration on the size of synthesized crystals and layer thickness. (b) High magnification SEM image highlighting the shape of an individual HAp crystal for sample with the highest concentration of NH_4OH .

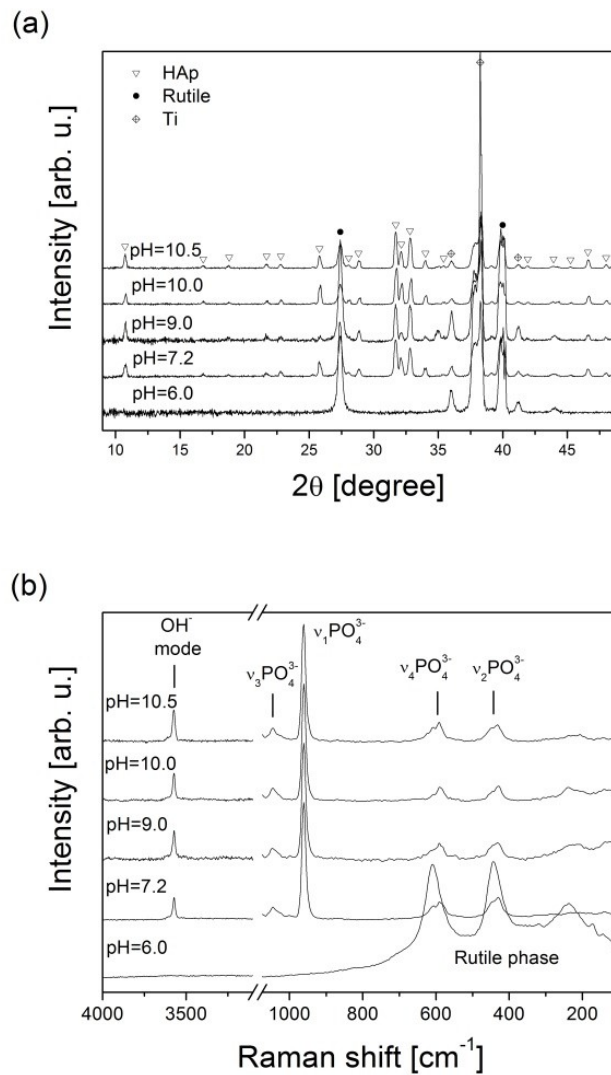


Figure 3. (a) XRD patterns and (b) Raman spectra of HAp crystals synthesized at different NH_4OH concentrations on titanium substrate.

The XRD results were confirmed by Raman spectroscopy (Figure 3b). Samples synthesized at pH = 6.0 revealed Raman bands characteristic only for titanium oxide in rutile phase [34]. For other samples we observed the characteristic bands for HAp phase [35], i.e., vibrations of PO_4^{3-} groups observed in the position of $390\text{--}470\text{ cm}^{-1}$ (ν_2 mode assigned to the doubly degenerate bending vibration of O–P–O bonds), $560\text{--}625\text{ cm}^{-1}$ (ν_4 frequency resulting from the triply degenerate bending mode of O–P–O bonds), 961 cm^{-1} (ν_1 mode assigned to the symmetric stretching vibration of P–O bond), $1010\text{--}1100\text{ cm}^{-1}$ (ν_3 mode attributed to the triply degenerate stretching vibration of P–O bonds), and OH^- symmetric stretching mode in the high wavenumber region at 3575 cm^{-1} .

More details of the chemical composition of our samples were obtained by PIXE method. A unique opportunity offered by PIXE measurements is a non-destructive determination of the element concentration within a sample up to ppm level. PIXE offers high element sensitivities for transition elements with medium atomic mass and for that reason it is a very useful tool for monitoring changes in concentration of calcium phosphates [36]. Figure 4 shows the comparison of PIXE spectra obtained for the HAp coatings grown at different pH values. Peaks at energies 2.013 keV and 3.692 keV indicate K_α lines of phosphorous and calcium, respectively. In addition, the strong peaks observed between 4 and 5 keV energy, and weak peak around 2.7 keV, testify to the presence of titanium. The results show the presence of both calcium and phosphorous species in all examined samples, even samples synthesized at pH = 6.0. The quantity of Ca and P for sample synthesized at lowest pH was relatively small and was significantly enhanced when the pH increased. The reduction of titanium contribution was also detected. PIXE spectra demonstrate that the content of calcium and phosphorus in the samples increases with pH, which indirectly indicates an increase in the amount of the hydroxyapatite phase. These data confirm prior observations, showing the increase of HAp thickness with the increasing ammonia concentration.

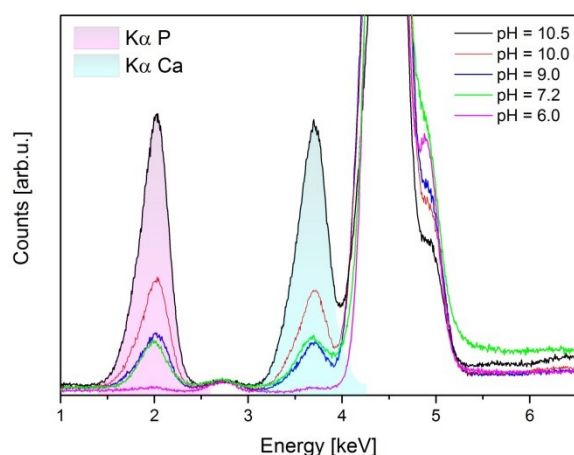


Figure 4. PIXE results for titanium samples hydrothermally treated in calcium phosphate solution with various pH.

4. Discussion

To date, crystallization of HAp by chelate decomposition method has allowed to control the morphology of powders. The pH changes of reaction solution were carried out by various alkalinizing agents, such as NaOH, KOH or NH_4OH [20,21,24,25]. It was shown that increasing the pH leads to a reduction in particles size. Arce et al. presented a shape evolution from plate like monetite at pH = 5.0 to the tiny elongated HAp specimens at pH = 9.0 [21]. Chen et. al. synthesized fluorapatite crystals with various morphologies in the presence of different chelating reagents at various pH conditions [20]. They showed that the shape of the particles evolved from flower-like crystals at pH = 3.6 to nanowires at pH = 10.0. Similar results were obtained by Lak et al., who synthesized at pH = 12 dandelion-like

HAp nanostructures with high specific surface area [13]. The size reduction of crystals is explained on the basis of selective adsorption of OH^- ions under high pH conditions.

The morphology of crystals grown during heterogeneous crystallization of coatings is controlled not only by the chemicals involved in the reactions but also through the interface on which the apatite layer is deposited. The possibility of obtaining HAp coatings on various metallic substrates using chelate decomposition synthesis route was first shown by Fujishiro et al. [24,25]. Since then, various seeding layers on the titanium substrate have been used in order to induce controlled growth of HAp crystals [26–28]. In the present study, we obtained hydroxyapatite coatings composed of hexagonal rods with a c-axis orientation using the appropriate concentration of NH_4OH directly on the titanium substrate. We also observed that there is pH of reaction solution below which the nucleation and subsequent HAp crystal growth are restrained. These results suggest that the use of strong chelating ligand, such as EDTA together with pH adjusting reagent, such as ammonia enables facile control over the morphology of HAp crystals grown on titanium substrate during hydrothermal process. In general, the driving force for crystallization from the solution is supersaturation, which under the hydrothermal conditions is controlled by the complexing compound, the initial pH of the solution and the temperature. Initially, EDTA wraps around the calcium ion to form a stable chelate ring and depletes the solution into free Ca^{2+} . The reduction of free Ca^{2+} ions induces an inhibitory effect on the nucleation of HAp. However, the tendency of the Ca-EDTA complex to dissociate in solutions increases with an increasing temperature. This means that with an increasing reaction temperature under hydrothermal conditions, the stability of Ca-EDTA complex is weakened and the Ca^{2+} ions are released into solution. Ca^{2+} ions then react with the negative phosphate and hydroxyl ions in the medium to form hydroxyapatite crystals. The stability of Ca-EDTA is also pH dependent and for an acidic environment, the chemical equilibrium is shifted towards complex dissociation, hence more calcium ions are released into the medium under given temperature condition. At high supersaturation the rapid nucleation generates a large number of nuclei which tend to grow to low dimension particles. In contrast, a low degree of supersaturation promotes crystal growth over nuclei formation. The slow growth rate causes the HAp crystal to form hexagonal rods due to intrinsic factor which is hexagonal symmetry of crystalline hydroxyapatite. This is the case of high concentrations of ammonia for which the stability of Ca-EDTA is enhanced.

In our research, the HAp crystals grow on the titanium substrate. Modification of titanium and formation of the oxide layer results in the appearance of functional groups such as $-\text{OH}$ which serve as active sites to promote the heterogeneous formation of HAp nuclei. However, at a solution of pH below 7, the HAp crystals on the titanium substrate did not grow. We speculate that this is due to the surface charge of titanium oxide in aqueous medium. The isoelectric point (IEP) for the surface of titanium oxide varies between 5.0 and 6.5 (depending on the crystal phase) [32]. This means that when the pH of solution is less than 6.5 the electrostatic interaction between the surface of the oxide and the ions in the medium is weakened, resulting in nucleation inhibition.

5. Conclusions

In conclusion, our study shows the effect of NH_4OH concentration (resulting in pH variations) on the hydrothermal crystal growth of hydroxyapatite directly on the Ti/ TiO_2 substrate without any additional seeding layer. We observe a pH limit for which the precipitation of HAp on titanium occurs. In acidic environments ($\text{pH} < 7$), this study shows that the crystals growth of HAp on Ti/ TiO_2 is inhibited. A further increase in pH ($\text{pH} > 7$) leads to the growth of HAp crystals on the Ti/ TiO_2 substrate. Crystal size and shape evolve from irregular plates into well-defined rods with hexagonal symmetry. Structural studies confirm the presence of hydroxyapatite. Our results also show that NH_4OH has a measurable influence on the coating thickness. With the increase of NH_4OH concentration we observe an increase in thickness of the HAp layer, also indicating an increase of the crystal growth rate. We demonstrate that the morphological and structural characteristics of crystals growth on the Ti/ TiO_2 surface can be controlled by a simple change of the pH of the starting solution.

Author Contributions: Conceptualization, K.S.; methodology, K.S., M.P. and J.L.; investigation, K.S. and M.S.; writing—original draft preparation, K.S.; writing—review and editing, K.S. and M.M.; supervision, M.M.

Funding: This research received no external funding.

Conflicts of Interest: The authors declare no conflict of interest.

References

1. Olszta, M.J.; Cheng, X.; Jee, S.S.; Kumar, R.; Kim, Y.Y.; Kaufman, M.J.; Douglas, E.P.; Gower, L.B. Bone structure and formation: A new perspective. *Mater. Sci. Eng. R* **2007**, *58*, 77–116. [[CrossRef](#)]
2. Dorozhkin, S.V. Calcium orthophosphate deposits: Preparation, properties and biomedical applications. *Mater. Sci. Eng. C* **2015**, *55*, 272–326. [[CrossRef](#)] [[PubMed](#)]
3. Bar-On, B.; Wagner, H.D. Structural motifs and elastic properties of hierarchical biological tissues—A review. *J. Struct. Biol.* **2013**, *183*, 149–164. [[CrossRef](#)] [[PubMed](#)]
4. Sadat-Shojai, M.; Khorasani, M.T.; Dinpanah-Khoshdargi, E.; Jamshidi, A. Synthesis methods for nanosized hydroxyapatite with diverse structures. *Acta Biomater.* **2013**, *9*, 7591–7621. [[CrossRef](#)] [[PubMed](#)]
5. Xu, H.; Geng, X.; Liu, G.; Xiao, J.; Li, D.; Zhang, Y.; Zhu, P.; Zhang, C. Deposition, nanostructure and phase composition of suspension plasma-sprayed hydroxyapatite coatings. *Ceram. Int.* **2016**, *42*, 8684–8690. [[CrossRef](#)]
6. Fomin, A.; Fomina, M.; Koshuro, V.; Rodionov, I.; Zakharevich, A.; Skaptsov, A. Structure and mechanical properties of hydroxyapatite coatings produced on titanium using plasma spraying with induction preheating. *Ceram. Int.* **2017**, *43*, 11189–11196. [[CrossRef](#)]
7. Mayr, H.; Ordnung, M.; Ziegler, G. Development of thin electrophoretically deposited hydroxyapatite layers on TiAl6V4 hip prosthesis. *J. Mater. Sci.* **2006**, *41*, 8138–8143. [[CrossRef](#)]
8. Nathanael, A.J.; Sabari Arul, N.; Ponpandian, N.; Mangalaraj, D.; Chen, P.C. Nanostructured leaf like hydroxyapatite/TiO₂ composite coatings by simple sol-gel method. *Thin Solid Films* **2010**, *518*, 7333–7338. [[CrossRef](#)]
9. Ivanova, A.A.; Surmeneva, M.A.; Surmenev, R.A.; Depla, D. Influence of deposition conditions on the composition, texture and microstructure of RF-magnetron sputter-deposited hydroxyapatite thin films. *Thin Solid Films* **2015**, *591*, 368–374. [[CrossRef](#)]
10. Suchanek, K.; Bartkowiak, A.; Gdowik, A.; Perzanowski, M.; Kac, S.; Szaraniec, B.; Suchanek, M.; Marszałek, M. Crystalline hydroxyapatite coatings synthesized under hydrothermal conditions on modified titanium substrates. *Mater. Sci. Eng. C* **2015**, *51*, 57e63. [[CrossRef](#)]
11. Roeder, R.K.; Converse, G.L.; Leng, H.; Yue, W. Kinetic effects on hydroxyapatite whiskers synthesized by the chelate decomposition method. *J. Am. Ceram. Soc.* **2006**, *89*, 2096–2104. [[CrossRef](#)]
12. Zhu, R.; Yu, R.; Yao, J.; Wang, D.; Ke, J. Morphology control of hydroxyapatite through hydrothermal process. *J. Alloys Compd.* **2008**, *457*, 555–559. [[CrossRef](#)]
13. Lak, A.; Mazloumi, M.; Mohajerani, M.; Kajbafvala, A.; Zanganeh, S.; Arami, H.; Sadrnezhaad, S.K. Self-assembly of dandelion-like hydroxyapatite nanostructures via hydrothermal method. *J. Am. Ceram. Soc.* **2008**, *91*, 3292–3297. [[CrossRef](#)]
14. Xie, R.; Feng, Z.; Li, S.; Xu, B. EDTA-Assisted self-assembly of fluoride-substituted hydroxyapatite coating on enamel substrate. *Cryst. Growth Des.* **2011**, *11*, 5206–5214. [[CrossRef](#)]
15. Neira, I.S.; Guitián, F.; Taniguchi, T.; Watanabe, T.; Yoshimura, M. Hydrothermal synthesis of hydroxyapatite whiskers with sharp faceted hexagonal morphology. *J. Mater. Sci.* **2008**, *43*, 2171–2178. [[CrossRef](#)]
16. Neira, I.S.; Kole'ko, Y.; Lebedev, O.I.; Van Tendeloo, G.; Gupta, H.S.; Guitian, F.; Yoshimura, M. Effective morphology control of hydroxyapatite crystals via hydrothermal synthesis. *Cryst. Growth Des.* **2009**, *9*, 466–474. [[CrossRef](#)]
17. Wu, S.C.; Tsou, H.K.; Hsu, H.C.; Hsu, S.K.; Liou, S.P.; Ho, W.F. A hydrothermal synthesis of eggshell and fruit waste extract to produce nanosized hydroxyapatite. *Ceram. Int.* **2013**, *39*, 8183–8188. [[CrossRef](#)]
18. Kimn, I.Y.; Ohtsuki, C. Hydroxyapatite formation from calcium carbonate single crystal under hydrothermal condition: Effects of processing temperature. *Ceram. Int.* **2016**, *42*, 1886–1890. [[CrossRef](#)]
19. Yan, L.; Li, Y.; Deng, Z.X.; Zhuang, J.; Sun, X. Surfactant-assisted hydrothermal synthesis of hydroxyapatite nanorods. *Int. J. Inorg. Mater.* **2001**, *3*, 633–637. [[CrossRef](#)]

20. Chen, M.; Jiang, D.; Li, D.; Zhu, J.; Li, G.; Xie, J. Controllable synthesis of fluorapatite nanocrystals with various morphologies: Effects of pH value and chelating reagent. *J. Alloys Compd.* **2009**, *485*, 396–401. [[CrossRef](#)]
21. Arce, H.; Montero, M.L.; Saenz, A.; Castano, V.M. Effect of pH and temperature on the formation of hydroxyapatite at low temperatures by decomposition of a Ca–EDTA complex. *Polyhedron* **2004**, *23*, 1897–1901. [[CrossRef](#)]
22. Taheri, M.M.; Abdul Kadir, M.R.; Shokuhfar, T.; Hamlekhan, A.; Assadian, M.; Shirdar, M.R.; Mirjalili, A. Surfactant-assisted hydrothermal synthesis of Fluoridated Hydroxyapatite nanorods. *Ceram. Int.* **2015**, *41*, 9867–9872. [[CrossRef](#)]
23. Tombacz, E. pH-dependent surface charging of metal oxides. *Period. Polytech. Chem. Eng.* **2009**, *53*, 77. [[CrossRef](#)]
24. Fujishiro, Y.; Sato, T.; Okuwaki, A. Coating of hydroxyapatite on metal plates using thermal dissociation of calcium-EDTA chelate in phosphate solutions under hydrothermal conditions. *J. Mater. Sci. Mater. Med.* **1995**, *6*, 172–176. [[CrossRef](#)]
25. Fujishiro, Y.; Fujimoto, A.; Sato, T.; Okuwaki, A. Coating of hydroxyapatite on titanium plates using thermal dissociation of Calcium-EDTA Chelate Complex in phosphate solutions under hydrothermal conditions. *J. Colloid Interface Sci.* **1995**, *173*, 119–127. [[CrossRef](#)]
26. Lu, Z.Z.; Xu, H.Y.; Xin, M.D.; Li, K.W.; Wang, H. Induced growth of (0001)-oriented hydroxyapatite nanorod arrays on ZnO-seeded glass substrate. *J. Phys. Chem. C* **2010**, *114*, 820–825. [[CrossRef](#)]
27. Chen, W.; Long, T.; Guo, Y.-J.; Zhu, Z.-A.; Guo, Y.-P. Hydrothermal synthesis of hydroxyapatite coatings with oriented nanorod arrays. *RSC Adv.* **2014**, *4*, 185. [[CrossRef](#)]
28. Shen, J.; Qi, Y.; Jin, B.; Wang, X.; Hu, Y.; Jiang, Q. Control of hydroxyapatite coating by self-assembled monolayers on titanium and improvement of osteoblast adhesion. *J. Biomed. Mater. Res. B Appl. Biomater.* **2017**, *105*, 124–135. [[CrossRef](#)]
29. Li, H.; Mei, L.; Liu, H.; Liu, Y.; Liao, L.; Kumar, R.V. Growth mechanism of surfactant-free size-controlled luminescent hydroxyapatite nanocrystallites. *Cryst. Growth Des.* **2017**, *17*, 2809–2815. [[CrossRef](#)]
30. Kokubo, T.; Pattanayak, D.K.; Yamaguchi, S.; Takadama, H.; Matsushita, T.; Kawai, T.; Takemoto, M.; Fujibayashi, S.; Nakamura, T. Positively charged bioactive Ti metal prepared by simple chemical and heat treatment. *J. R. Soc. Interface* **2010**, *7*, 503–513. [[CrossRef](#)]
31. Pattanayak, D.K.; Yamaguchi, S.; Matsushita, T.; Nakamura, T.; Kokubo, T. Apatite forming ability of titanium in terms of pH of the exposed solution. *J. R. Soc. Interface* **2012**, *9*, 2145–2155. [[CrossRef](#)]
32. Kosmulski, M. Compilation of PZC and IEP of sparingly soluble metal oxides and hydroxides from literature. *Adv. Colloid. Interface Sci.* **2009**, *152*, 14–25. [[CrossRef](#)]
33. Koutsopoulos, S. Synthesis and characterization of hydroxyapatite crystals: A review study on the analytical methods. *J. Biomed. Mater. Res.* **2002**, *62*, 600–612. [[CrossRef](#)]
34. Hardcastle, F.D.; Ishihara, H.; Sharma, R.; Biris, A.S. Photoelectroactivity and Raman spectroscopy of anodized titania (TiO₂) photoactive water-splitting catalysts as a function of oxygen-annealing temperature. *J. Mater. Chem.* **2011**, *21*, 6337–6345. [[CrossRef](#)]
35. Tsuda, H.; Arends, J. Orientational micro-Raman spectroscopy on hydroxyapatite single crystals and human enamel crystallites. *J. Dent. Res.* **1994**, *73*, 1703–1710. [[CrossRef](#)]
36. Heimann, R.B.; Ntsoane, T.P.; Pineda-Vargas, C.A.; Przybylowicz, W.J.; Topić, M. Biomimetic formation of hydroxyapatite investigated by analytical techniques with high resolution. *J. Mater. Sci. Mater. Med.* **2008**, *19*, 3295–3302. [[CrossRef](#)]

